Space Weather

RESEARCH ARTICLE
10.1029/2019SW002305

Special Section:
Scientific Challenges of Space Weather Forecasting Including Extremes

On the Annual Asymmetry of High-Latitude Sporadic F

Alex T. Chartier[1], J. D. Huba[1], and Cathryn N. Mitchell[2]

[1]Johns Hopkins University Applied Physics Laboratory, Laurel, MD, USA, [2]Department of Electronic & Electrical Engineering, University of Bath, Bath, UK

Abstract The polar *F* region ionosphere frequently exhibits sporadic variability (e.g., Meek, 1949, https://doi.org/10.1029/JZ054i004p00339; Hill, 1963, https://doi.org/10.1175/1520-0469(1963)020<0492:SEOLII>2.0.CO;2). Recent satellite data analysis (Noja et al., 2013, https://doi.org/10.1002/rds.20033; Chartier et al., 2018, https://doi.org/10.1002/2017JA024811) showed that the high-latitude *F* region ionosphere exhibits sporadic enhancements more frequently in January than in July in both the northern and southern hemispheres. The same pattern has been seen in statistics of the degradation and total loss of GPS service onboard low-Earth orbit satellites (Xiong et al. 2018, https://doi.org/10.5194/angeo-36-679-2018). Here, we confirm the existence of this annual pattern using ground GPS-based images of TEC from the MIDAS algorithm. Images covering January and July 2014 confirm that the high-latitude (>70 MLAT) *F* region exhibits a substantially larger range of values in January than in July in both the northern and southern hemispheres. The range of TEC values observed in the polar caps is 38–57 TECU (north-south) in January versus 25–37 TECU in July. First-principle modeling using SAMI3 reproduces this pattern, and indicates that it is caused by an asymmetry in plasma levels (30% higher in January than in July across both polar caps), as well as 17% longer O^+ plasma lifetimes in northern hemisphere winter, compared to southern hemisphere winter.

Plain Language Summary The polar *F* region ionosphere frequently exhibits sporadic variability. Satellite data analysis has indicated an annual pattern to this variability—there appears to be more sporadic *F* in January than in July in both hemispheres. The same pattern has been seen in statistics of GPS navigation system outages on low-Earth orbit satellites. Here we confirm that pattern exists throughout the *F* region using GPS data collected at ground stations in the northern and southern high latitudes. A numerical model reproduces the observations accurately. In the model, the annual pattern of variability is caused by two factors: (1) 30% higher plasma levels in January than in July across both polar caps and (2) 17% longer plasma lifetimes in northern winter than in southern winter.

Key Points:
- The high-latitude ionosphere is more variable in January than in July in both the northern and southern hemispheres
- First-principle modeling reproduces the patterns observed using GPS-derived TEC
- The pattern is caused by the annual ionospheric asymmetry and by the long plasma lifetimes found in northern hemisphere winter

Correspondence to:
A. T. Chartier,
alex.chartier@jhuapl.edu

Citation:
Chartier, A. T., Huba, J. D., & Mitchell, C. N. (2019). On the annual asymmetry of high-latitude sporadic F. *Space Weather*, *17*, 1618–1626. https://doi.org/10.1029/2019SW002305

Received 16 JUL 2019
Accepted 29 OCT 2019
Accepted article online 8 NOV 2019
Published online 29 NOV 2019

1. Introduction

1.1. High-Latitude Ionospheric Variability

Sporadic enhancements of *F* region ionization are frequently observed at high latitudes (e.g., Hill, 1963; Meek, 1949). Over the course of a few minutes, the bulk plasma density increases by up to an order of magnitude, typically accompanied by horizontal drift speeds in excess of 1 km/s and intense density structuring. This type of observation has been given several different names, including “patches” and “tongues of ionization.” It is now generally accepted that at least the large *F* region enhancements are made up of photoionized plasma convected into the polar caps from the subauroral dayside (e.g., Carlson, 2012). Recently, there has been controversy over the annual occurrence rate of this phenomenon, with Noja et al. (2013) first reporting that sporadic *F* region enhancements are seen more frequently in January than July in both hemispheres. Noja et al.'s (2013) conclusion is opposite to longstanding expectations of what happens in the southern hemisphere, where it was believed that there would be more enhancements in July (which is local winter there).

The prevailing argument over the last several decades has been that the high-latitude *F* region should appear less variable in local summer because the background ionization is much higher then and so the contrast is reduced (e.g.,Foster, 1989 ; Sojka et al., 1994). Notable observations that appear to support that theory include Coley and Heelis (1998) and Spicher et al. (2017), who counted more *F* region density

spikes in local winter in each hemisphere. Chartier et al. (2018) explained that the apparent contradiction between Noja et al. (2013) and the others is the result of different counting metrics: Noja et al. (2013) tested for a proxy of ΔN (topside TEC enhancements >4 TECU), whereas the typical approach has been to look for changes in $\Delta N/N$, expressed perhaps most famously in Crowley's (1996) test specifying that a patch must be greater than twice the background density. This choice of a different metric explains why Noja et al. (2013) got a different result than the others, but it does not explain why ΔN should have an annual variability with a marked minimum in July. Additionally, it should be noted that ΔN appears to be the more important quantity from a technological perspective: Xiong et al. (2018) showed that high-latitude GPS signal loss from low-Earth orbit (LEO) has the same annual variability as was seen by Noja et al. (2013) and Chartier et al. (2018).

Given these unexpected observations and the link to a major form of space weather, it is important to find the cause of this annual *F* region variability. It has been noted (e.g., by Xiong et al., 2018) that the pattern matches the well-known global ionospheric annual asymmetry, first reported by Berkner et al. (1936) and Berkner and Wells (1938). The ionospheric annual asymmetry constitutes a 20–40% increase in the global *F* layer plasma density in December/January compared to that in June/July (e.g.,Chartier et al., 2012 ; Mendillo et al., 2005 ; Rishbeth & Müller-Wodarg, 2006 ; Zeng et al., 2008). Another important factor to consider is the lifetime of plasma in the polar caps. Wood and Pryse (2010) have put forward the theory that reduced plasma lifetimes in the northern polar cap during summer explain the relative lack of ionospheric variability seen there. Their parameter estimation indicates that this effect is caused primarily by variation in the chemical composition of the atmosphere, which, in summer, both reduced the plasma density drawn into the polar cap and enhanced plasma loss by recombination.

2. Method

The goal of this investigation is to determine the annual pattern of sporadic high-latitude *F* region enhancements at large horizontal scales (hundreds of kilometers and larger), and to understand its causes. Ground-based GPS tomography provides the best observing platform due to its broad, continuous spatial coverage and widespread year-round availability. The ionospheric *F* layer is usually the densest and always the thickest layer, so it provides the dominant contribution to GPS TEC. Ground GPS also provides a contrast to the LEO satellite-based approaches that have been employed previously. Results from the SAMI3 model are used to understand whether these observations can be explained by current physical understanding (as constituted in the model).

Tomographic reconstructions of ionospheric electron density are produced using the University of Bath's Multi-Instrument Data Analysis Software (MIDAS; Mitchell & Spencer, 2003; Spencer & Mitchell, 2007). The algorithm applies a constrained nonlinear approach to observations taken by a global network of dual-frequency GPS receivers. Electron density images are integrated vertically to obtain ionospheric Total Electron Content (TEC), whose dominant contribution comes from the *F* region electron density. In the present configuration, the horizontal grid extent is ~300 km (northern hemisphere) and ~500 km (southern hemisphere due to reduced data coverage there), with the grid covering all latitudes >45°. Data coverage is good in both polar caps, although there are large gaps in the oceans in the southern hemisphere. Poorly resolved regions of the images are removed from the analysis using the adaptive resolution mapping technique described in Chartier et al. (2012).

The SAMI3 model (Huba et al., 2000; Huba et al., 2008) is used to assess whether our observations are consistent with current physical understanding of the ionosphere. SAMI3 solves for the dynamic plasma and chemical evolution of seven ion species (H^+, He^+, N_2^+, O^+, N^+, NO^+, and O_2^+) on a field-aligned magnetic apex coordinate grid extending up to 87° MLAT. Photoionization is calculated using solar flux from the Flare Irradiance Spectral Model by Chamberlin et al. (2008), which is driven by Solar Dynamics Observatory Extreme Ultraviolet Variability Experiment data. SAMI3 contains a self-consistent electric potential solver that is seamlessly combined with an imposed high-latitude potential from Weimer's (2005) model (driven by solar wind parameters observed by the Advanced Composition Explorer). The Hardy model (Hardy et al., 1985, 1989) provides auroral electron and ion precipitation estimates based on the K_P index. The neutral atmosphere is specified by the Horizontal Wind Model 2014 by Drob

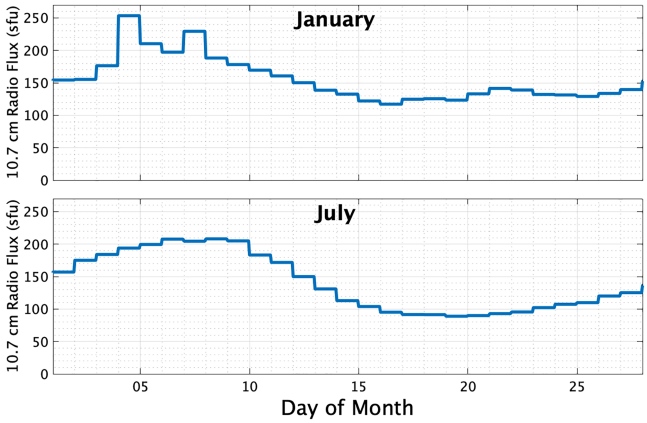

Figure 1. shows $F_{10.7}$ Solar flux levels observed at Penticton, Canada during January and July 2014. The mean in January is 155, whereas the mean in July is 141.

et al. (2015) and the Naval Research Laboratory's Mass Spectrometer Incoherent Scatter Model 2000 of neutral atmospheric densities by Picone et al. (2002). These drivers represent statistically average estimates of conditions based on historical data sets and globally defined input drivers. Therefore, SAMI3 is not expected to provide accurate instantaneous predictions, but can provide insights into climatological behavior.

The year 2014 is chosen for analysis because it is the most recent year of high solar activity, when ionospheric variability is known to be larger. Output is produced for 1–28 January and July to cover the most pronounced part of the annual asymmetry identified in Chartier et al. (2018). These two periods had a similar range of insolation, as approximated by the $F_{10.7}$ index, as can be seen from Figure 1. Likewise geomagnetic activity is similar, with both periods exhibiting low to moderate levels of activity. To provide a geophysical reference point, the apex magnetic coordinate system (Richmond, 1995), referenced at 300-km altitude, is used to identify 60° and 70° MLAT bounds within the images. The zone poleward of 70° MLAT is considered to be the polar cap for this investigation.

The first step is to test Noja et al.'s (2013) conclusions regarding the annual variability of $\mathbf{\Delta N}$. This is achieved by determining the median, range, and standard deviation of TEC values from the MIDAS observations and SAMI3 model in both polar caps (up to 87° MLAT for direct comparison between model and observations) in January and July 2014. The median TEC serves as a proxy for average F region density, N, while the range captures the extremes of polar F region variability, referred to hereafter as $\mathbf{\Delta N}$. The range is calculated as maximum-minimum of TEC values observed or modeled in each polar cap over each month. We emphasize that range is not necessarily representative of the variability of the whole population of polar TEC values, which is indicated by the standard deviation. Rather, the range provides information on sporadic F region enhancements, which are the target of this investigation.

The second step is to calculate the plasma lifetime in the model. The lifetime is defined as the average time an ion exists before undergoing charge exchange or recombining. Since this investigation focuses on the F region, where O^+ dominates, the O^+ lifetime is used. At a point location, the O^+ lifetime, τ, is simply the inverse of its loss rate Ψ (which occurs through charge exchange or recombination). For diagnostic purposes, the O^+ lifetime is integrated from 200–400-km altitude, weighted according to the O^+ density at each point, and averaged across the polar cap. This calculation is shown in equation (1).

$$\tau = \frac{\int N_{O+}.\partial h}{\int \Psi.N_{O+}.\partial h} \tag{1}$$

The equations used to calculate the O^+ loss rate Ψ can be found in section 6 of Huba et al. (2000). The loss rate depends on the number density of molecular neutral species (O_2 and N_2) available for charge exchange, as well as a weak dependence on ion temperature.

3. Results

Figure 2 shows an example of high-latitude TEC from MIDAS and SAMI3 in both hemispheres at 19 UT on 23 January 2014. In the northern hemisphere, enhanced TEC enters the polar cap as a tongue of ionization from the Canadian sector, which is just postnoon in this image. In the southern hemisphere, a similar tongue of ionization forms from a somewhat later UT sector (note that the Earth's rotation appears counterclockwise in the north but clockwise in the south). Agreement between model and

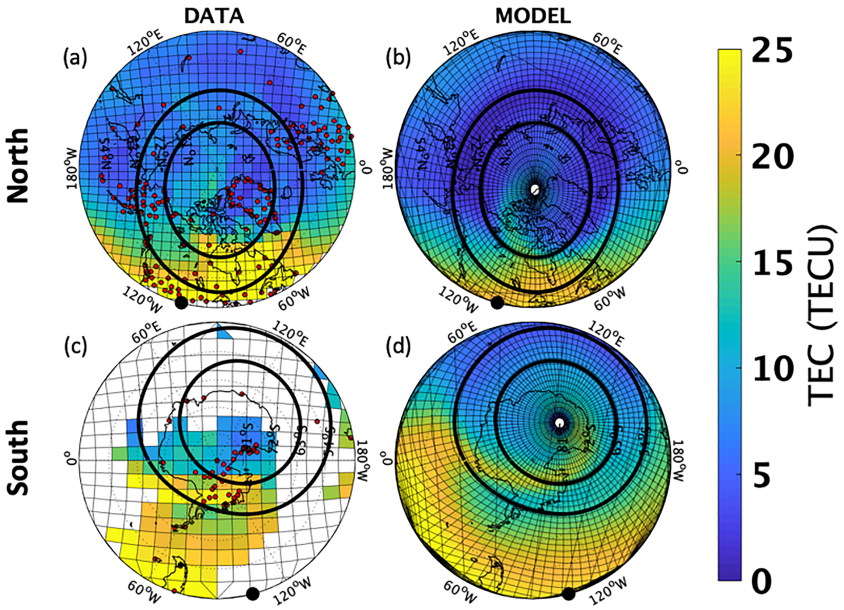

Figure 2. High-latitude TEC from (a and c) MIDAS and (b and d) SAMI3 at 19 UT on 1 January 2014. Black rings show 60° and 70° MLAT (at 300-km apex). Black dots at perimeter indicate local noon. Red dots indicate GPS ground stations.

observations appears to be good in both hemispheres, given the limitations of data coverage and of model drivers.

Figure 3 shows 19 UT on 23 July 2014, to allow for direct comparison to Figure 2. In this case, average TEC values are about the same as in Figure 2 in the north but values are much lower in the south. However, polar cap TEC variability is much reduced in both hemispheres: the values are almost uniform above 70 MLAT. Once again agreement between model and data is good in the polar caps.

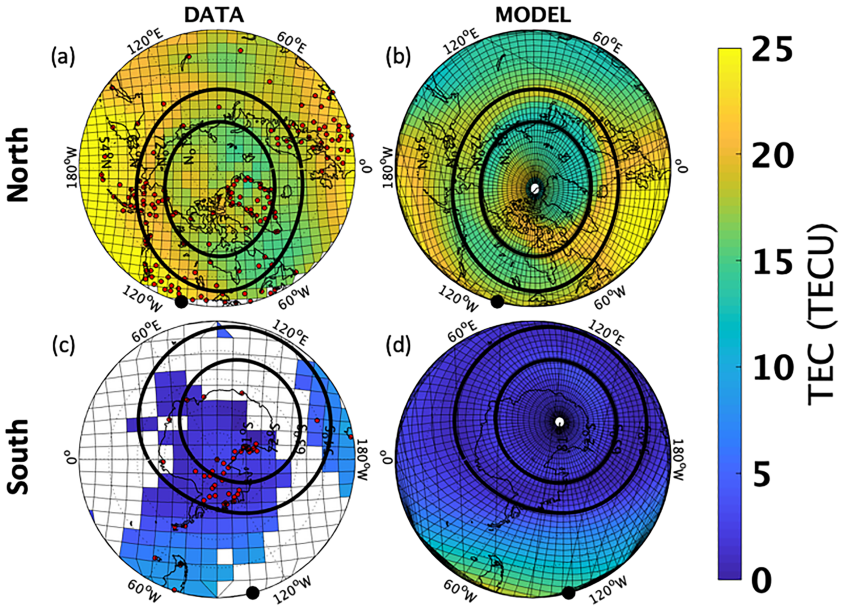

Figure 3. High-latitude TEC from (a and c) MIDAS and (b and d) SAMI3 at 19 UT on 1 July 2014. Black rings show 60° and 70° MLAT (at 300-km apex). Black dots at perimeter indicate local noon. Red dots indicate GPS ground stations.

Table 1
Medians, Standard Deviations, and Ranges of 70–87 MLAT TEC From MIDAS Data and SAMI3 Model

	Hemisphere	MIDAS median/standard/range (TECU)	SAMI3 median/standard/range (TECU)
January	North	5.4/3.4/37.8	4.5/2.7/22.4
	South	18.2/6.1/57.1	19.2/6.4/36.9
July	North	14.9/3.7/24.6	14.4/3.6/19.4
	South	3.3/4.3/36.9	4.3/3.7/21.0

To quantify TEC variability in the polar caps, we perform a statistical assessment of all the MIDAS and SAMI3 TEC values between 70 and 87 MLAT for 1–28 January and July 2014. Means and ranges for each month are provided in Table 1.

The model is consistent with the data in most regards, showing similar median values (within 1 TECU in all cases) and the same trends across all three statistical measures, although the data show a much larger range of values.

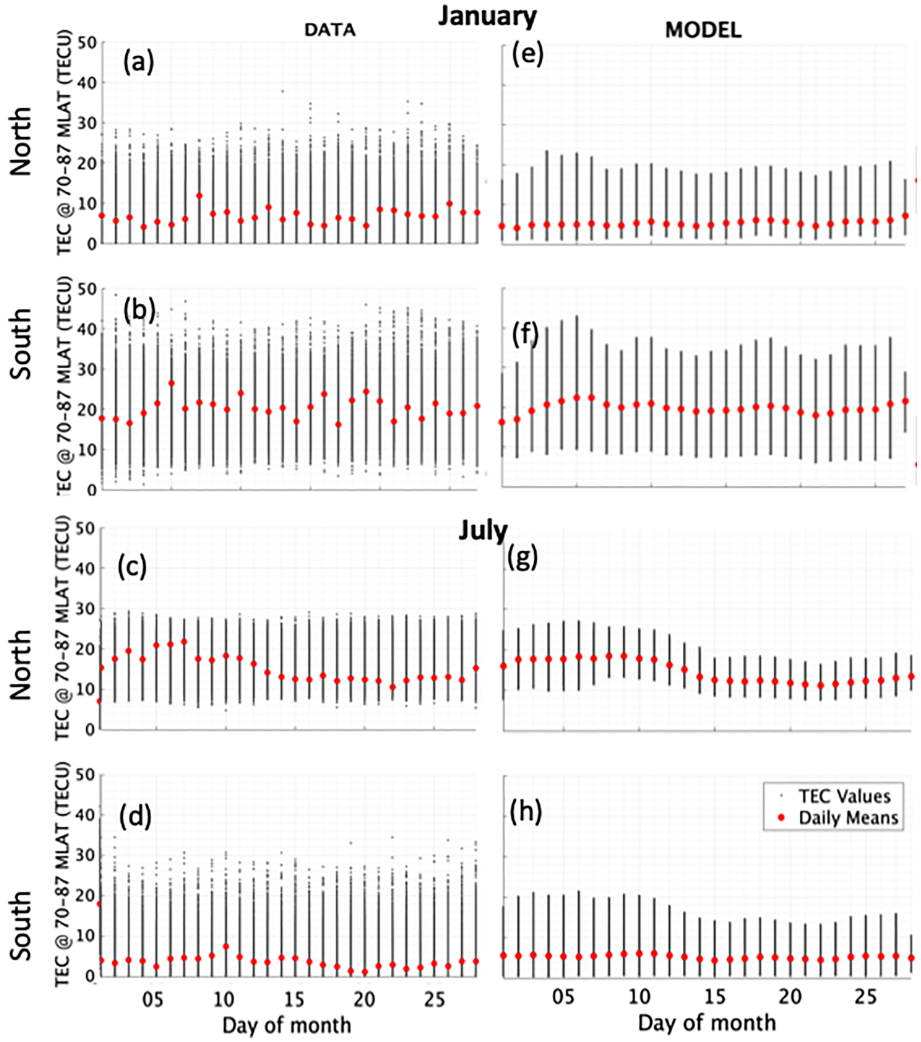

Figure 4. TEC values between 70 and 87 MLAT north and south (defined at 300-km magnetic apex) from (a–d) MIDAS and (e–h) SAMI3. Daily means are overlaid in red. Means are higher in summer, while ranges are larger in January.

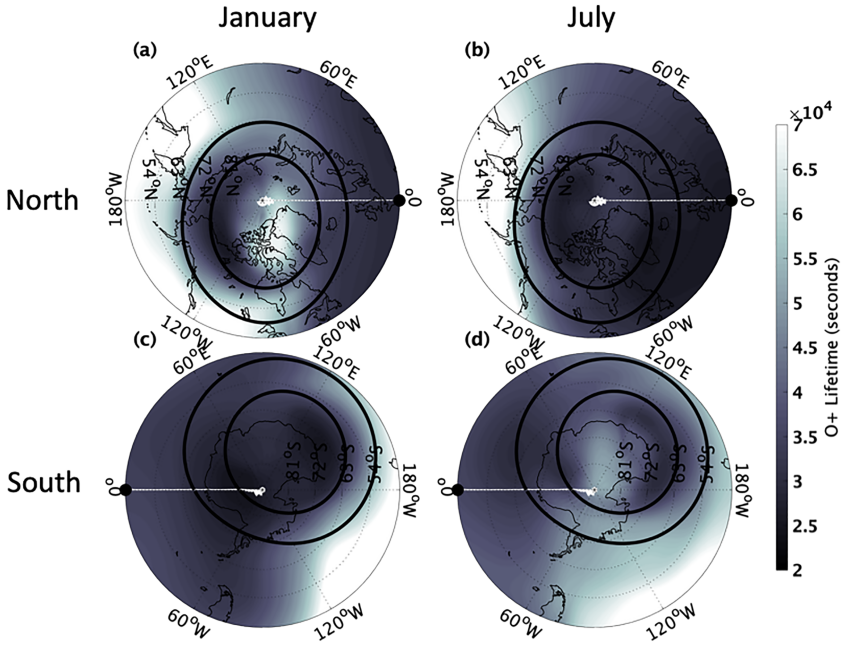

Figure 5. The 200–400-km averaged O^+ lifetimes at 12 UT on 24 January and July 2014. Local noon is shown as a black dot on the perimeter. The 60 and 70 MLAT are shown as black rings. Lifetimes are (a) longest in northern winter and (b and c) shortest in the summer cases.

The results in Table 1 show that the southern polar cap is far more variable than the north, both in terms of seasonal swings and within each month. By far the highest median, standard deviation, and range are observed in southern hemisphere summer (22%, 41%, and 51% larger than the next-highest values observed). Related to this, the well-known global annual asymmetry in ionospheric plasma levels is also present in this polar cap data: the combined January medians are 30% higher than in July in the data (27% higher in the model). The annual asymmetry reinforces local seasonal swings in the south and counteracts them in the north.

As is to be expected, the medians are always higher in local summer than in local winter, and the standard deviations follow this seasonal pattern. However, surprisingly, the ranges are always larger in January than in July. The northern polar cap has a larger range of TEC values in winter despite the fact that the median and standard deviation are smaller than in summer.

Figure 4 shows a daily breakdown of the data from which these statistics were drawn.

These results confirm that $\Delta \boldsymbol{N}$ is larger in January than in July in both polar caps, and that the SAMI3 model reproduces this variability. Considering that $\boldsymbol{N}$ is higher in local summer, it might be expected that $\Delta \boldsymbol{N}$ should also be higher then. From that perspective, the northern hemisphere is actually the anomalous one. Wood and Pryse (2010) found that $\Delta \boldsymbol{N}$ is suppressed in northern hemisphere summer primarily because of decreased plasma lifetimes found there. To quantify this effect in our SAMI3 runs, we calculated the average O^+ plasma lifetimes between 200–400 km and 70–87 MLAT. An example of this quantity is shown in Figure 5.

Table 2
Average O^+ Lifetimes Between 70–87 MLAT and 200–400 km From SAMI3 Model

	January lifetimes (s)	July lifetimes (s)
North	4816	3089
South	2932	4120

Inside the polar caps, O^+ lifetimes are longest in northern winter and shorter in local summer in both hemispheres. Generally, O^+ lifetimes are anticorrelated with neutral temperature (e.g., shorter lifetimes are seen around noon and in local summer) due to the upwelling of molecular neutral species that occurs when temperatures are higher. Monthly averaged O^+ lifetimes are shown in Table 2.

Winter O^+ lifetimes are 17% longer in the northern hemisphere, whereas summer lifetimes are 5% longer in the northern

hemisphere. This hemispheric asymmetry is a contributing factor in the different seasonal patterns seen in both hemispheres. The density of O_2 and N_2 in the *F* region is the most important variable in determining these lifetimes.

4. Discussion

GPS-derived images of the high-latitude ionosphere in both hemispheres confirm the pattern first observed by Noja et al. (2013): sporadic *F* region variability ($\Delta \boldsymbol{N}$) is larger in January than in July in both hemispheres. These observations provide the first ground-based confirmation of that surprising pattern, refuting any suggestion that it is merely the result of topside scale height variations or an accident of LEO satellite observational coverage. This pattern has now been observed using three types of instrument (LEO upward GPS, Langmuir Probe, ground-based GPS tomography) and over 10 years (2001–2004 and 2013–2018). For several decades, the prevailing theory has been that the high-latitude *F* region appears less variable in local summer than in winter due to reduced contrast against higher ambient levels of ionization. While ambient ionization ($\boldsymbol{N}$) is higher in local summer (and therefore $\Delta \boldsymbol{N}/\boldsymbol{N}$ is smaller in summer than in winter), the contrast theory is clearly incomplete in that it does not explain the observed variation of $\Delta \boldsymbol{N}$.

Here we show that the pattern of $\Delta \boldsymbol{N}$ being larger in January than in July in both hemispheres is successfully modeled by SAMI3 driven by climatological inputs (FISM photoionization, Weimer convection, HWM neutral winds, MSIS neutral atmosphere). The ultimate driver of this behavior appears to be a combination of several factors. A priori, we might expect $\Delta \boldsymbol{N}$ to be larger when $\boldsymbol{N}$ is larger. From that perspective, the southern hemisphere behavior is as expected ($\Delta \boldsymbol{N}$ larger in local summer) and the northern hemisphere is anomalous in that $\Delta \boldsymbol{N}$ is larger in local winter. We have identified two factors that contribute to this anomalous behavior:

1. The ionospheric annual asymmetry (~30% more plasma present in January than in July) extends to the polar caps. Averaged across both polar caps, 30% higher TEC is observed in January as compared to July. This effect counteracts seasonal variations in the north and reinforces them in the south.
2. Modeling indicates that O^+ lifetimes are especially long in northern winter, around 17% higher than in southern winter. Therefore, sporadic enhancements of the polar *F* region last longer in northern winter than elsewhere.

Given that sporadic *F* region enhancements are made up of photoionized plasma convected into the polar caps from the subauroral dayside (e.g., Carlson, 2012), the well-known global annual asymmetry (e.g., Mendillo et al., 2005 ; Rishbeth & Müller-Wodarg, 2006) also plays an important role in driving the observed pattern of variability, as it controls plasma levels in the supply region. These factors combine in SAMI3 to reproduce the pattern of variability observed here and by Noja et al. (2013) and Chartier et al. (2018), with ΔN (as characterized by the range of TEC values present in the polar cap) larger in January than in July in both hemispheres.

By far the highest densities and most variable conditions were observed in southern summer—the mean, standard deviation, and range of TEC values there were 22%, 41%, and 51% larger than the next-highest values observed, respectively. This is in part because the annual asymmetry reinforces seasonal variations in the southern hemisphere, but also because the southern magnetic pole is displaced further from the geographic pole than is the case in the north (15° versus 7° in 300-km apex coordinates). This larger offset of the south magnetic pole allows denser plasma (from lower geographic latitudes) to enter the polar convection pattern in the southern hemisphere.

5. Conclusions

Ground GPS-based TEC observations from 2014 indicate that the ionosphere poleward of 70 MLAT has a larger range of values in January than in July in both hemispheres. First-principle modeling reproduces the observed variability using standard climatological drivers. The pattern of variability in the southern hemisphere directly contradicts the longstanding theory that the high-latitude ionosphere is more variable in local winter. From the alternative perspective that $\Delta \boldsymbol{N}$ should vary proportionally to $\boldsymbol{N}$, the northern hemisphere is actually the anomalous one. Our model analysis indicates that the pattern observed arises

because of an asymmetry in winter plasma lifetimes (17% longer in northern winter than in southern winter) and 30% higher electron densities in January as compared with July.

Appendix A

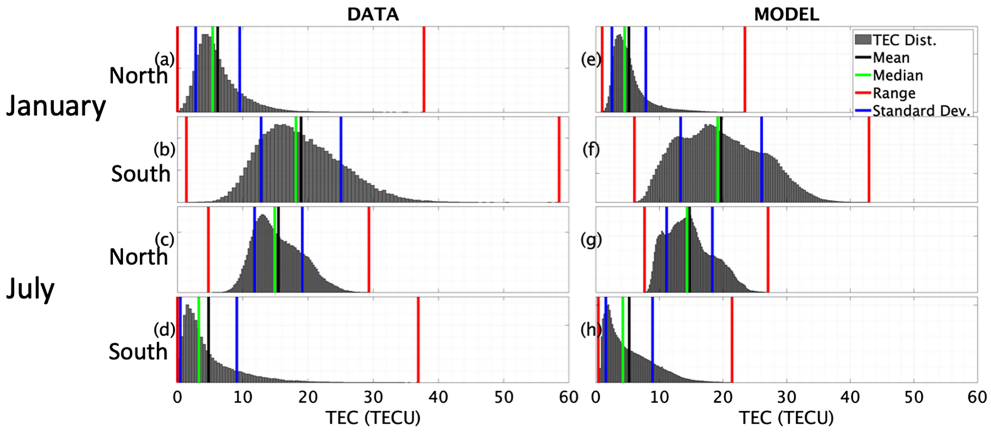

Figure A1. Distributions and statistical characteristics of TEC values between 70-87 MLAT in January and July 2014. MIDAS GPS-derived data on the left (a-d) and SAMI3 model on the right (e-h). The model shows the same trends as the data, although the range of values is larger in the data. Means, medians and standard deviations are larger in local summer, whereas ranges are large in January in both hemispheres due to long tails of large values.

Acknowledgments
A.T.C. and J.D.H. acknowledge support from National Science Foundation grants OPP-1643773 and AGS-1341885. C.N.M. acknowledges support from NERC grant fellowship NE/P006450/1. The raw GPS data used in this paper are available at ftp://garner.ucsd.edu, ftp://geodesy.noaa.gov, and ftp://data-out.unavco.org. The precise orbit files are also available at ftp://garner.ucsd.edu. Advanced Composition Explorer data, K_P, $F_{10.7}$, and sunspot number are available at omniweb.gsfc.nasa.gov. Flare Irradiance Spectral Model data are available at lasp.colorado.edu/lisird/data/fism. The SAMI3 and MIDAS output shown in this paper is available at zenodo.org/record/3406247 and zenodo.org/record/3445409.

References

Berkner, L. V., & Wells, H. W. (1938). Non-seasonal change of F_2 region ion density. *Terrestrial Magnetism and Atmospheric Electricity*, *43*, 15–36. https://doi.org/10.1029/TE043i001p00015

Berkner, L. V., Wells, H. W., & Seaton, S. L. (1936). Characteristics of the upper region of the ionosphere. *Terrestrial Magnetism and Atmospheric Electricity*, *41*, 173–184. https://doi.org/10.1029/TE041i002p00173

Carlson, H. C. (2012). Sharpening our thinking about polar cap ionospheric patch morphology, research, and mitigation techniques. *Radio Science*, *47*, RS0L21. https://doi.org/10.1029/2011RS004946

Chamberlin, P. C., Woods, T. N., & Eparvier, F. G. (2008). Flare irradiance spectral model (FISM): Flare component algorithms and results. *Space Weather*, *6*, S05001. https://doi.org/10.1029/2007SW000372

Chartier, A. T., Mitchell, C. N., & Jackson, D. R. (2012). A 12 year comparison of MIDAS and IRI 2007 ionospheric Total Electron Content. *Advances in Space Research*, *49*(9), 1348–1355.

Chartier, A. T., Mitchell, C. N., & Miller, E. S. (2018). Annual occurrence rates of ionospheric polar cap patches observed using Swarm. *Journal of Geophysical Research: Space Physics*, *123*, 2327–2335. https://doi.org/10.1002/2017JA024811

Chartier, A. T., Smith, N. D., Mitchell, C. N., Jackson, D. R., & Condor, P. J. (2012). The use of ionosondes in GPS ionospheric tomography at low latitudes. *Journal of Geophysical Research*, *117*, A10326. https://doi.org/10.1029/2012JA018054

Coley, W. R., & Heelis, R. A. (1998). Seasonal and universal time distribution of patches in the northern and southern polar caps. *Journal of Geophysical Research*, *103*(A12), 29,229–29,237.

Crowley, G. (1996). Critical review of ionospheric patches and blobs. *Review of Radio Science 1993–1996* (pp. 619–648).

Drob, D. P., Emmert, J. T., Meriwether, J. W., Makela, J. J., Doornbos, E., Conde, M., et al. (2015). An update to the Horizontal Wind Model (HWM): The quiet time thermosphere. *Earth and Space Science*, *2*, 301–319. https://doi.org/10.1002/2014EA000089

Foster, J. C. (1989). Plasma Transport through the Dayside Cleft: A Source of Ionization Patches in the Polar Cap. In P. E. Sandholt, & A. Egeland (Eds.), *Electromagnetic Coupling in the Polar Clefts and Caps. NATO ASI Series (C: Mathematical and Physical Sciences)*, (Vol. 278, pp. 343–354). Dordrecht: Springer.

Hardy, D. A., Gussenhoven, M. S., & Brautigam, D. (1989). A statistical model of auroral ion precipitation. *Journal of Geophysical Research*, *94*(A1), 370–392.

Hardy, D. A., Gussenhoven, M. S., & Holeman, E. (1985). A statistical model of auroral electron precipitation. *Journal of Geophysical Research*, *90*(A5), 4229–4248.

Hill, G. E. (1963). Sudden enhancements of *F*-layer ionization in polar regions. *Journal of the Atmospheric Sciences*, *20*(6), 492–497. https://doi.org/10.1175/1520-0469(1963)020<0492:SEOLII>2.0.CO;2

Huba, J. D., Joyce, G., & Fedder, J. A. (2000). Sami2 is Another Model of the Ionosphere (SAMI2): A new low-latitude ionosphere model. *Journal of Geophysical Research*, *105*(A10), 23,035–23,053.

Huba, J. D., Joyce, G., & Krall, J. (2008). Three-dimensional equatorial spread F modeling. *Geophysical Research Letters*, *35*, L19106. https://doi.org/10.1029/2009GL040284

Meek, J. H. (1949). Sporadic Ionization at High Latitudes. *Journal of Geophysical Research*, *54*(4).

Mendillo, M., Huang, C.-L., Pi, X., & Rishbeth, H. (2005). Meier, The global ionospheric asymmetry in total electron content. *Journal of Atmospheric and Solar-Terrestrial Physics*, *67*(15), 1377–1387. https://doi.org/10.1016/j.jastp.2005.06.021

Mitchell, C. N., & Spencer, P. S. J. (2003). A three-dimensional time-dependent algorithm for ionospheric imaging using GPS. *Annales Geophysicae*, *46*(4), 687.

Noja, M., Stolle, C., Park, J., & Lühr, H. (2013). Long-term analysis of ionospheric polar patches based on CHAMP TEC data. *Radio Science*, *48*, 289–301. https://doi.org/10.1002/rds.20033

Picone, J. M., Hedin, A. E., Drob, D. P., & Aikin, A. C. (2002). NRLMSISE-00 empirical model of the atmosphere: Statistical comparisons and scientific issues. *Journal of Geophysical Research*, *107*(A12), 1468. https://doi.org/10.1029/2002JA009430

Richmond, A. D. (1995). Ionospheric electrodynamics using magnetic apex coordinates. *Journal of Geomagnetism and Geoelectricity*, *47*, 191–212.

Rishbeth, H., & Müller-Wodarg, I. C. F. (2006). Why is there more ionosphere in January than in July? The annual asymmetry in the F2-layer. *Annales Geophysicae*, *24*(12), 3293–3311.

Sojka, J. J., Bowline, M. D., & Schunk, R. W. (1994). Patches in the polar ionosphere: UT and seasonal dependence. *Journal of Geophysical Research*, *99*, 14,959–14,970. https://doi.org/10.1029/93JA03327

Spencer, P. S. J., & Mitchell, C. N. (2007). Imaging of fast moving electron-density structures in the polar cap, Ann. *Geophysical*, *50*(3), 427–434.

Spicher, A., Clausen, L. B. N., Miloch, W. J., Lofstad, V., Jin, Y., & Moen, J. I. (2017). Interhemispheric study of polar cap patch occurrence based on Swarm in situ data. *Journal of Geophysical Research: Space Physics*, *122*, 3837–3851. https://doi.org/10.1002/2016JA023750

Weimer, D. R. (2005). Predicting surface geomagnetic variations using ionospheric electrodynamic models. *Journal of Geophysical Research*, *110*, A12307. https://doi.org/10.1029/2005JA011270

Wood, A. G., & Pryse, S. E. (2010). Seasonal influence on polar cap patches in the high-latitude nightside ionosphere. *Journal of Geophysical Research*, *115*, A07311. https://doi.org/10.1029/2009JA014985

Xiong, C., Stolle, C., & Park, J.-H. (2018). Climatology of GPS signal loss observed by Swarm satellites. *Annales Geophysicae*, *36*(2), 679–693. https://doi.org/10.5194/angeo-36-679-2018

Zeng, Z., Burns, A., Wang, W., Lei, J., Solomon, S., Syndergaard, S., et al. (2008). Ionospheric annual asymmetry observed by the COSMIC radio occultation measurements and simulated by the TIEGCM. *Journal of Geophysical Research*, *113*, A07305. https://doi.org/10.1029/2007JA012897